Sensors and Actuators B 228 (2016) 634–642

Contents lists available at ScienceDirect

Sensors and Actuators B: Chemical

journal homepage: www.elsevier.com/locate/snb

Superior triethylamine-sensing properties based on TiO_2/SnO_2 n–n heterojunction nanosheets directly grown on ceramic tubes

Hongyan Xu*, Judianxing Ju, Wenru Li, Jun Zhang, Jieqiang Wang, Bingqiang Cao*

School of Materials Science and Engineering, Laboratory of Inorganic Energy and Environment Materials, Shandong Provincial Key Laboratory of Preparation and Measurement of Building Materials, University of Jinan, Jinan 250022, Shandong, China

ARTICLE INFO

Article history:
Received 6 August 2015
Received in revised form
31 December 2015
Accepted 14 January 2016
Available online 16 January 2016

Keywords:
SnO_2 nanosheets
TiO_2
n–n Heterojunctions
Triethylamine
Depletion layer

ABSTRACT

A highly sensitive and selective gas sensor towards triethylamine (TEA) has been successfully fabricated by designing n–n heterojunctions consisting of SnO_2 nanosheets and TiO_2 nanoparticles. The SnO_2 nanosheets with the thickness about 15 nm were directly grown on Al_2O_3 ceramic tubes by a simple hydrothermal process. After the formation of n–n heterojunctions by employing PLD method, the TiO_2 nanoparticle/SnO_2 nanosheets heterojunctions exhibit high sensing properties to TEA gas. The as-prepared ST3 (SnO_2/TiO_2 3000) sensor response could reach to 52.3 at relatively low temperature (260 °C) when exposed to 100 ppm TEA gas, which is much higher than that of pure SnO_2 nanosheet sensor (~3@100 ppm TEA@320 °C). Compared with the pure SnO_2 nanosheet sensor (S sensor), the depletion layer formed at the n–n heterojunctions interface in TiO_2/SnO_2 sensor can greatly increase the resistance in air and decrease the resistance in TEA gas. Due to the general working principle and controllable growth strategy, this work provides a way for developing the chemiresistive gas sensors.

© 2016 Elsevier B.V. All rights reserved.

1. Introduction

Triethylamine (TEA), a colorless transparent liquid with a strong ammonia-like odor, has been widely used as solvents, catalysts and raw materials in the process of organic synthesis. It can also be secreted in dead fish and sea creatures. The TEA concentration can increases with the decay of the dead fish and marine products. Taking its volatility, highly combustible and toxicity into account, TEA can result in serious damage to human health and environment, such as eye and skin chemical burns caused by contacting. TEA can also cause pulmonary edema and even death on inhalation [1,2]. Although, several methods have been adopted to detect TEA, such as chromatography, electrochemistry analysis, and colorimetric method [3–5], the reference electrodes and expensive equipment hinder their application [6]. Thus, there is a great demand for accurate and fast detection of TEA with high sensitivity and good selectivity in biomedical, chemical, food industries and our daily life.

SnO_2 is a chemically and thermally stable n-type oxide semiconductor with a wide band gap of 3.6 eV at room temperature [7–9]. It has been well reported that both the shape and size of materials can greatly influence the sensing properties of SnO_2 [10]. Thus, considerable efforts have been made to fabricate nanostructured SnO_2, such as nanoparticles, nanorods, nanosheets, and hollow spheres [11–15], in order to further improve its sensing performance. Among the various nanostructures, nanosheets have been paid great attention due to their high surface area to volume ratio and stability [14,16,17].

It is well known that SnO_2-based gas sensors exhibit good sensing properties to many flammable and explosive gases like trimethylamine (TMA) [18], CO and CH_4 [19]. However, SnO_2-based gas sensors for detecting TEA are rarely reported. To the best of our knowledge, only Wang et al [20] fabricated SnO_2 nanorods TEA sensor using the traditional slurry-coating method. However, the high working temperature (350 °C), low response (200@1000 ppm), and complex preparation process made it need further researched [20]. Recently, doping or formation of heterojunction has been demonstrated to be another way to improve the sensing properties [2,19,21–23]. By varying the electronic structure of the metal oxide nanocomposites, the inherent characteristics of the sensor can be tailored for detection of specific gases [21,22]. For example, Zhang et al. [22] have demonstrated by using Fe_2O_3@ZnO core–shell nanostructure as a model to improve the gas sensing properties. The electronic interaction between the metal oxide semiconductor components plays an important role in tuning the conductivity and sensor properties. Hsu et al. [23] synthesized high density vertical

* Corresponding authors. Fax: +86 531 87974453.
E-mail addresses: mse_xuhy@ujn.edu.cn (H. Xu), mse_caobq@ujn.edu.cn (B. Cao).

http://dx.doi.org/10.1016/j.snb.2016.01.059
0925-4005/© 2016 Elsevier B.V. All rights reserved.

Ti doped ZnO (ZnO:Ti) nanorods (NRs) to detect ethanol gas. The ethanol gas responses of the ZnO:Ti NRs are higher than that of the ZnO NRs by around 5.1 times to 1000 ppm ethanol. Our group fabricated NiO/ZnO pn heterojunctions gas sensor to detect TEA gas, and the sensor exhibited highly sensitive and selective sensing property to TEA gas [24].

In addition, as an n-type semiconductor with a wide bandgap of 3.2 eV [25]. TiO_2 (titanium dioxide) has been well known and used as an important gas sensing material because of its reversible and large changes in the electrical resistance and the exceptional chemical stability. There are some reports on high efficiency gas sensors based on TiO_2 [26–28]. Among them, there are several reports on the fabrication of heterojunction based on TiO_2 with high selectivity and response in recent years [27,28]. For example, Deng et al. used nanofibers of zinc oxide and titanium dioxide to fabricate (ZnO/TiO_2) heterojunction device for ethanol sensing. The ZnO/TiO_2 heterojunction showed higher response (~3 times) than only ZnO and TiO_2 based devices toward ethanol (20–500 ppm) [29].

In this paper, we have successfully implanted TiO_2 nanoparticles onto the surface of SnO_2 nanosheets by pulsed laser deposition (PLD) process. It is worth highlighting that the SnO_2 nanosheets synthesized directly on the Al_2O_3 tubes which can be used directly for gas sensor fabrication without the slurry-coating fabrication process. With the formation of n–n heterojunction, the sensitivity and selectivity of TiO_2/SnO_2 nanosheet sensor were enhanced obviously in comparison with pure SnO_2 nanosheet sensor and the possible sensing mechanism was also discussed.

2. Experimental

2.1. Direct growth of SnO_2 nanosheets on Al_2O_3 ceramic tubes

All the chemicals were purchased from Sinopharm Chemical Reagent (Shanghai, China). SnO_2 nanosheets were prepared by the following hydrothermal process: 0.04 M $SnCl_2{\cdot}2H_2O$ solution was mixed with 0.04 M $CO(NH_2)_2$ solution under stirring, and then they were transferred into Teflon-lined stainless steel autoclaves. At the same time, the cleaned Al_2O_3 tubes with predesigned gold electrodes were suspended into the aqueous solution. After the reaction at 95 °C for 24 h, we got the nanosheet samples. Then, SnO_2 nanosheets were obtained by further annealing the precipitation precursor in a muffle furnace at 500 °C for 4 h.

2.2. Growth of TiO_2 nanoparticles onto SnO_2 nanosheets by PLD

A layer of TiO_2 nanoparticles was deposited onto the surface of SnO_2 nanosheets by pulsed laser deposition (PLD) using TiO_2 target at room temperature. A KrF laser of 1 mJ/cm^2 and an oxygen partial pressure of 3×10^{-4} Pa were typically applied. By controlling the laser pulses, e.g., 1000, 2000, 3000, 4000 pulses, the TiO_2/SnO_2 nanosheet heterojunction with TiO_2 nanoparticle layer of different thickness were grown. Thus, different gas sensors directly fabricated with SnO_2 nanosheets, named as S sensor, and TiO_2/SnO_2 nanosheet heterojunction, named as ST1-ST4 sensor, were ready for further measurement.

2.3. Material characterizations and sensor properties

The morphology, microstructure, and composition of TiO_2/SnO_2 nanosheets were measured by a field emission scanning electron microscope (FESEM, FEI QUANTA FEG250) equipped with an energy dispersive X-ray spectroscopy (EDS, INCA MAX-50) and a high-resolution transmission electron microscope (HRTEM, JEM-2100F, JEOL) with an energy dispersive X-ray spectroscopy (EDX, OXFORD LINK-ISIS). The phase of the sensor materials was characterized by X-ray diffraction (XRD, D8-Advance, Bruker). X-ray photoelectron spectrum (XPS) analysis was conducted using an Al KaX-ray source (1486.6 eV) on a Thermo-VG ESCALAB MKII spectrometer. The gas sensing properties were measured by a gas sensing test system (WS-30A, Weisheng Electronics, Zhengzhou, China). The concentrations of the target gases were obtained by the static gas distribution method, which was calculated by the following Formula [30]:

$$Q = \frac{V \times \varphi \times M}{22.4 \times d \times \rho} \times 10^{-9} \times \frac{273 + T_R}{273 + T_B} \quad (1)$$

where Q (mL) is the liquid volume of the volatile compound, V (mL) is the volume of the testing chamber, φ is the required gas volume fraction, M (g mol^{-1}) is the molecular weight, d (g cm^{-3}) is the specific gravity, and ρ is the purity of the volatile testing liquid, T_R and T_B (°C) are the temperatures at ambient and test chamber, respectively. The devices were put into an airproof test box. Test gases of TEA with calculated concentration were injected into the testing chamber by a microsyringe. At a certain TEA concentration, the corresponding response of the sensor increases rapidly and reaches its equilibrium. Once the target gas is removed, the response decreases quickly to the baseline. The sensor response is defined as the ratio of R_a/R_g, where R_a and R_g are the resistances of the sensors in air and in target gas, respectively. The response and recovery time was defined as the time needed for the sensor-resistance to change by 90% of the difference from the maximum after injecting and removing the detected gas.

3. Results and discussion

3.1. Characterizations of SnO_2 and TiO_2/SnO_2 nanosheets

Fig. 1(a) is an optical photograph of an Al_2O_3 tube grown with SnO_2 nanosheets, interdigitated with a pair of Au electrodes, Pt lead wires and heater. The surface morphology of the SnO_2 nanosheets directly synthesized on the Al_2O_3 tubes is shown in Fig. 1(b). The optical photograph of the panorama device is shown in Fig. S1 (a) in supplementary information. However, due to the SnO_2 nanosheets were grown directly on the surface of the Al_2O_3 tube, it is difficult to be observed by naked eyes. Therefore, the FESEM measurement was carried out to observe the surface structure information of the sensing material on the surface of the Al_2O_3 tube, which was shown in Fig. S1 (b) and (c) in supplementary information. It can be seen that the thickness of SnO_2 nanosheets is about 15 nm. It has been reported that the sensing properties could remarkably increase as the average crystallite size decreases down to 20 nm [14,31,32]. This is because when the crystallite size is smaller than or close to twice the thickness of electron depletion layer, the whole particle can be fully depleted of electrons through surface interactions, which lead to the increase of the sensing properties [32]. Additionally, 2D structures are considered to be stable [33,34]. They are effective in mitigating the strong agglomeration between nanostructures. Moreover, the SnO_2 nanosheets distribute vertically on the Al_2O_3 tube, which will provide a larger contact area to the target gas. Fig. 1(c), (e), and (g) show the morphology of the SnO_2 nanosheets when a thin layer of TiO_2 nanoparticles was deposited onto their surface by PLD with laser pulses of 1000, 3000 and 4000, respectively. Fig. 1(d), (f) and (h) are the corresponding EDS spectrum of the TiO_2/SnO_2 samples. The peak of Ti can be clearly observed in all the spectra. According to the EDS analysis shown in inset of Fig. 1(b, d and f), it can be concluded that the TiO_2 content increases with the increasing laser pulses. The peaks of Al observed in the spectra are attributed to the Al_2O_3 tube.

The phases of the SnO_2 and TiO_2/SnO_2 nanosheets were tested by XRD. Fig. 2(a) exhibits the XRD spectrum of the SnO_2 nanosheets.

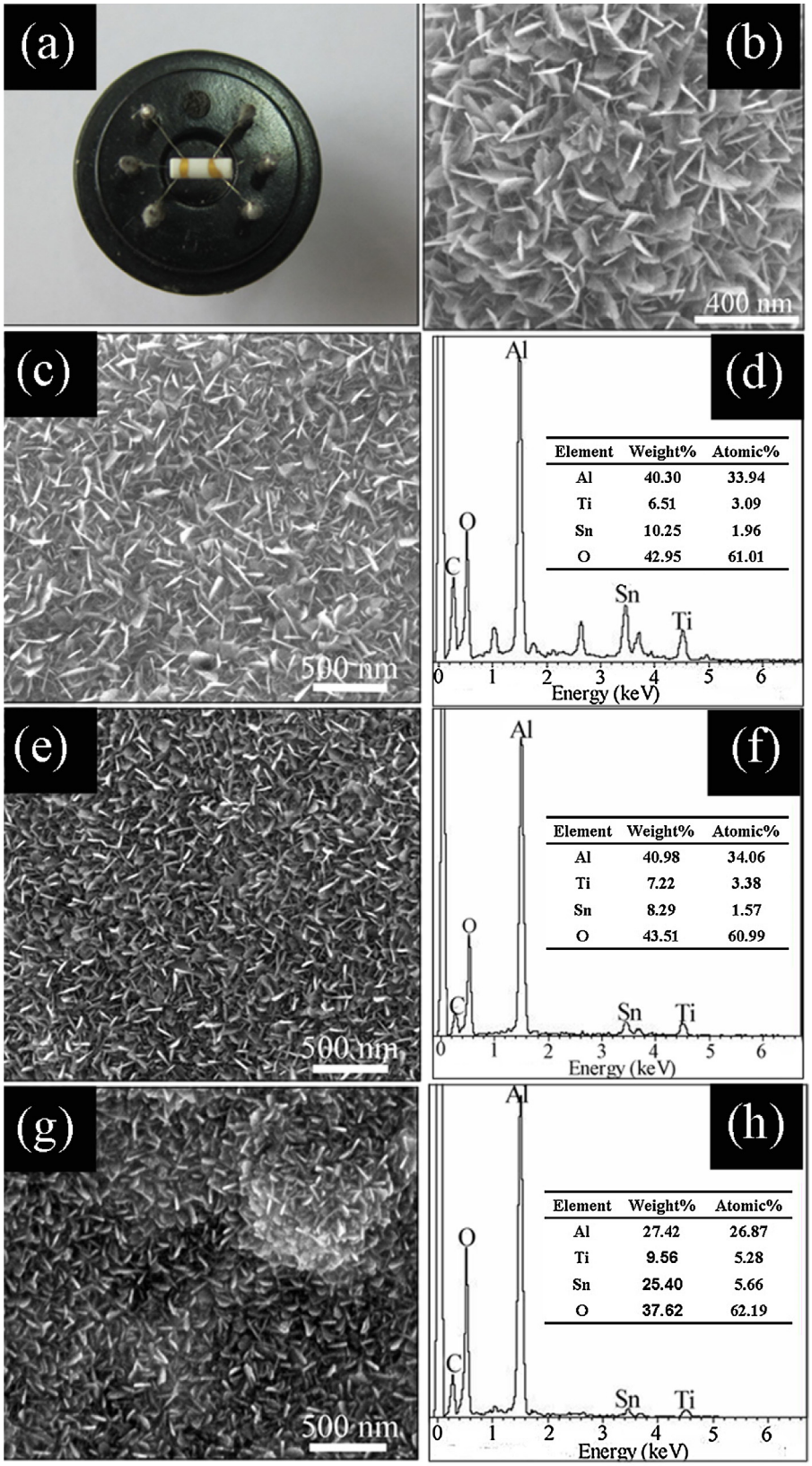

Fig. 1. (a) Gas sensor of SnO_2 nanosheets fixed on an electronic bracket; (b) SEM image of SnO_2 nanosheets taken from (a); SEM images and the corresponding EDS spectra of SnO_2 nanosheets after a PLD growth process for TiO_2 with different deposition laser pulses. ((c) and (d)) 1000 pulses; ((e) and (f)) 3000 pulses; ((g) and (h)) 4000 pulses.

Typical tetragonal rutile SnO_2 (JCPDS Card No. 41-1445) diffraction patterns can be observed with the diffraction peaks of under Al_2O_3 substrate. The weak peaks of TiO_2 (JCPDS card No. 88-1175) are due to the small amount.

To gain further insights into the crystallographic features of the pure SnO_2 nanosheets and the TiO_2/SnO_2 nanosheets, TEM, HRTEM and the associated diffraction techniques were employed, as shown in Fig. 3. Fig. 3(a) presents a TEM image for SnO_2 nanosheets. The

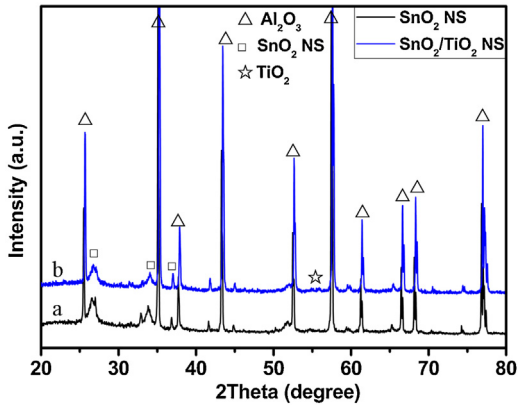

Fig. 2. XRD spectra of as-synthesized nanosheets grown on Al_2O_3 substrate. (a) SnO_2 nanosheets; (b) TiO_2/SnO_2 nanosheets with 3000 pulses.

inset SAED pattern indicates that the nanosheet is of polycrystalline structure composed of small nanoparticles. Fig. 3(b) shows the same HRTEM image, where the lattice spacings are determined to be 0.335 nm, corresponding to the (1 1 0) planes of the SnO_2. Fig. 3(c) is the EDX spectrum of the SnO_2 nanosheets. The peaks of Sn and O can be clearly observed in the spectrum.

TEM, HRTEM and diffraction analyses were also conducted for TiO_2/SnO_2. Fig. 3(d and e) shows the TEM and HRTEM images of TiO_2/SnO_2 nanosheets, where the lattice spacings are determined to be 0.335 nm of SnO_2 (1 1 0) and 0.188 nm of TiO_2 (2 0 0), respectively. The HRTEM image evidently demonstrates that TiO_2 nanoparticles are present on the surface of SnO_2 and form the n–n heterojunction. The EDX further demonstrates the TiO_2/SnO_2 composite is composed of Ti, Sn and O, as shown in Fig. 3(f).

The chemical composition and purity of the sample TiO_2/SnO_2 composite was also investigated by XPS analysis. The fully scanned spectra (Fig. 4a) demonstrates that Ti, Sn, O, and C exist in TiO_2/SnO_2 heterostructures. The C element can be ascribed to the adventitious carbon-based contaminant, and the binding energy for the C1s peak at 284.6 eV is used as the reference for calibration. Fig. 4(b) displays the high resolution Sn 3d spectra of this sample. Both Sn $3d_{5/2}$ and Sn $3d_{3/2}$ peaks are found to be asymmetric. Binding energy of Sn $3d_{5/2}$ was similar to that of Sn^{4+} in SnO_2 (486.6 eV), and higher than that of Sn^{2+} in SnO (485.9 eV) or Sn metal [35,36]. It is suggested that tin ions are positively charged by forming direct bonds with oxygen ions [35]. Besides, the peaks for Ti 2p in the composite show no shift compared with that in bare TiO_2, confirming that the structure of TiO_2 remains intact after synthesis of SnO_2 nanoparticles. In Fig. 4(c), there are two peaks in the Ti 2p region. The peak located at 464.2 eV corresponds to the Ti 2p1/2 and another one located at 458.5 eV is assigned to Ti 2p3/2. The splitting between Ti 2p1/2and Ti 2p3/2 is 5.7 eV, indicating a normal state of Ti^{4+} in the as-prepared TiO_2/SnO_2 heterostructures. The main component of O1s signal shown in Fig. 4(d), centered at 531.5 eV, is attributed to the lattice oxygen as O^{2-} in SnO_2 and TiO_2.

3.2. Performance comparison of S and ST sensors

Firstly, the gas sensing properties of the sensors were measured at different working temperature. Fig. 5 shows the response of the sensors to 100 ppm TEA as a function of the working temperature in the range of 200–400 °C. The optimal operating temperature for our sensors is around 260 °C and the response of ST3 sensor is much higher than that of other sensors in the whole temperature range. The sensor responses can reach 10 (ST3 sensor) even the temperature is lower than 200 °C. Furthermore, the response further increases with the increase of working temperature. When the temperature is up to 260 °C, the ST3 sensor exhibits the maximum response of 52.3. Then, the response decreases as the temperature further increases, which is due to the competing desorption of the chemisorbed oxygen [37,38]. When the working temperature is up to 260 °C, the chemical adsorption oxygen absorbed on the surface of the TiO_2/SnO_2 nanosheets will gain enough energy to desorb from the surface of nanosheets, and then the chemical adsorption of

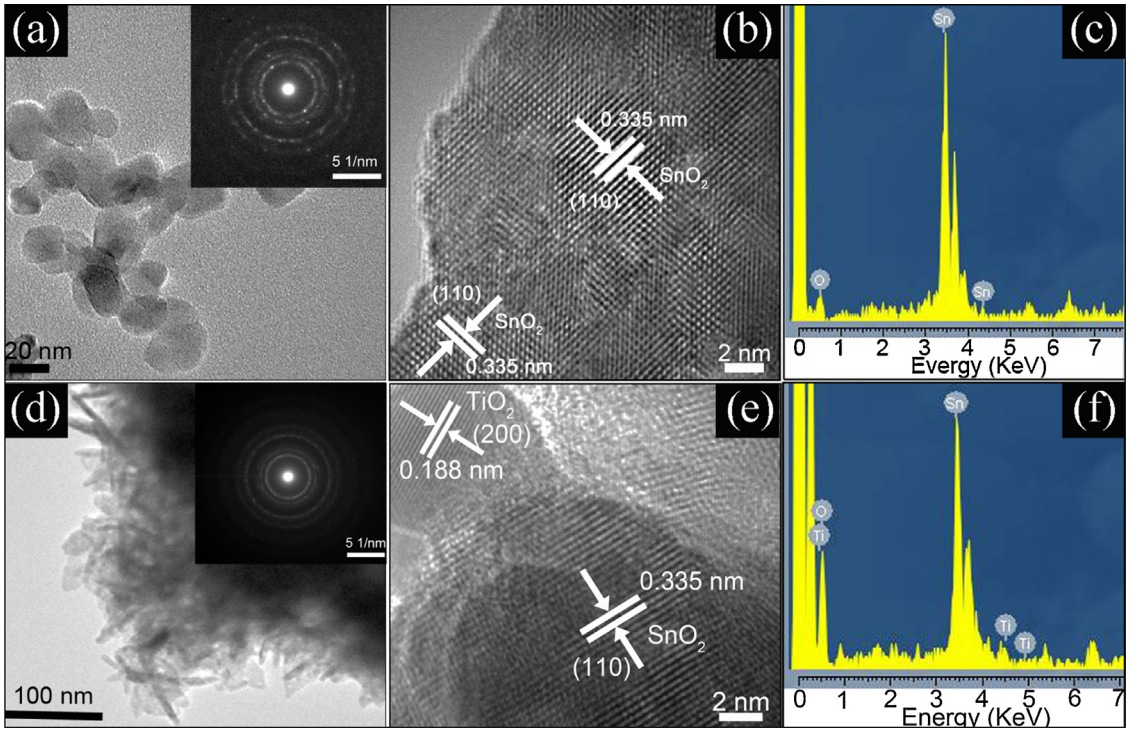

Fig. 3. (a–c) TEM, HRTEM, and EDS images of SnO_2 nansheets; (d–f) TEM, HRTEM, and EDS image of TiO_2/SnO_2 nanosheets.

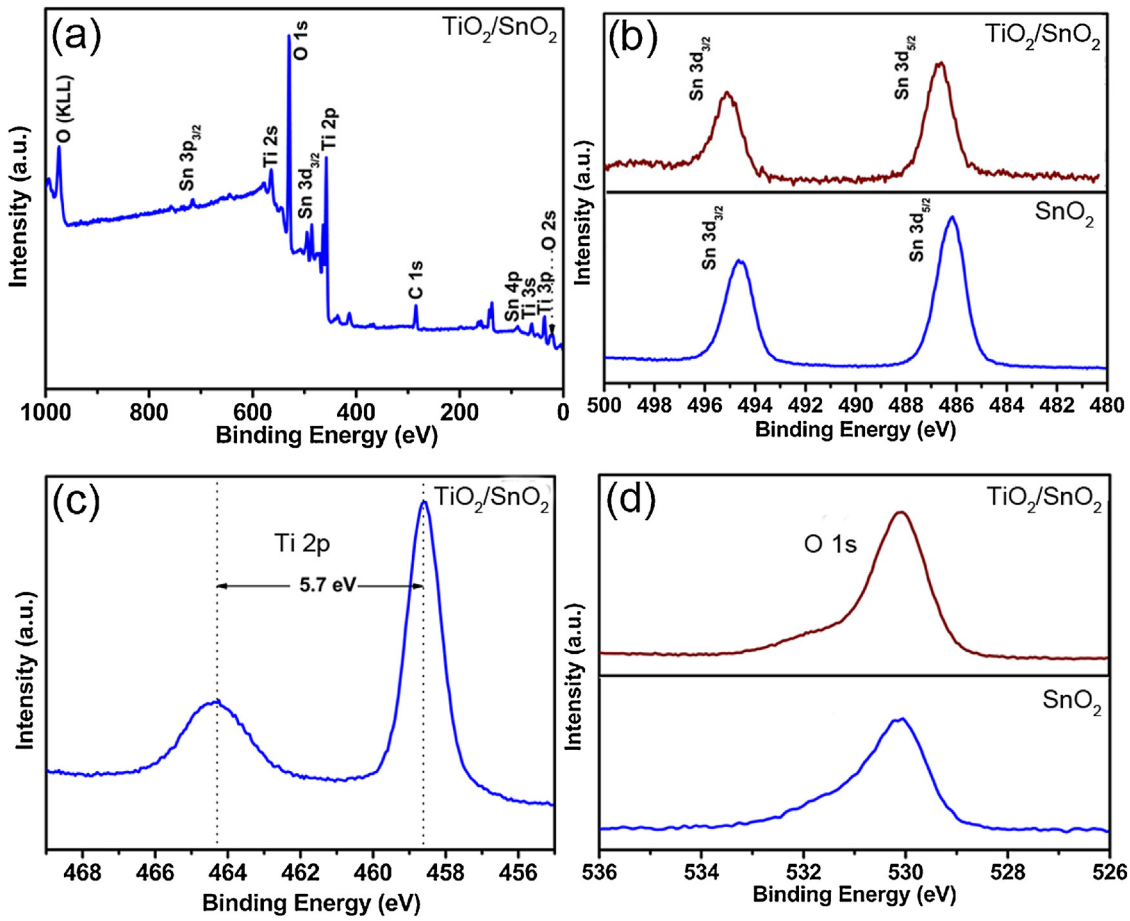

Fig. 4. XPS patterns of the as-synthesized TiO_2/SnO_2 sample: (a) XPS full spectrum; (b) Sn 3d spectra; (c) Ti 2p spectra; (d) O 1s spectra.

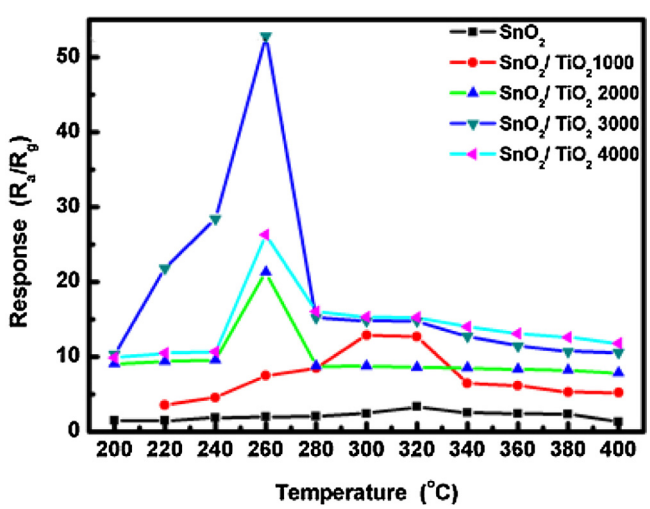

Fig. 5. The relationship between working temperature and response of SnO_2 sensor (S sensor) and TiO_2/SnO_2 sensors (ST sensors) to 100 ppm TEA gas.

oxygen gets saturation. With the further increase of operating temperature, the rate of desorption of target molecules is much higher than that of adsorption. This limits the reaction between adsorption oxygen and target gas molecules, which reduces the sensing response [39,40].

The sensor resistance in air and 50 ppm TEA of different sensors was shown in Fig. S2 in supplementary information. It can be seen that the resistance of SnO_2/TiO_2 3000 in air (ST3 > ST2 > S) was largest in the three kinds of sensors. This may be due to the formation of n–n heterojunctions. These results are also in agreement with the gas sensing mechanism later.

Fig. 6(a) indicates a typical response profile to investigate the repeatability of the gas sensors after aged for 3 days. It is noted that both the sensors are in good reproducible run after six cycles, indicating a very good repeatability of the sensors. Fig. 6(b) shows the response curve of the sensors to TEA gas of different concentrations from 2 to 1000 ppm at 260 °C. It is obvious that the sensor ST3 exhibits higher response than that of sensor S for higher TEA concentration in the range of 2–1000 ppm, which can be attributed to the formation of TiO_2/SnO_2 n–n heterojunctions. The sensor response of ST3 increases gradually with the increasing concentration of TEA and can reach to 140 when the TEA concentration is 1000 ppm. It also indicates that the response could reach to about 8 with a much lower concentration of 2 ppm.

The response/recovery time is another important parameter used for characterizing the sensor performance. According to the definition of response and recovery time, it can be clearly observed from Fig. 7(a) and (b) that when the target gas was injected into the box, both sensors response fast and the response time of sensor S and ST3 is 12 and 16 s, respectively. After evacuation, sensor S needs 35 s to recover the initial state, which is longer than that of sensor ST3 (22 s).

For the further optimized TiO_2/SnO_2 heterostructures, all the sensors shows a clear increase in the range of 10–100 ppm, with the increase of TEA concentration, as shown in Fig. 8(a). The cross response of the sensors were examined by exposing the sensors to 100 ppm TEA, ethanol, acetone, glycol, paraxylene at 260 °C, as summarized in Fig. 8(b). The ST3 sensor response to those

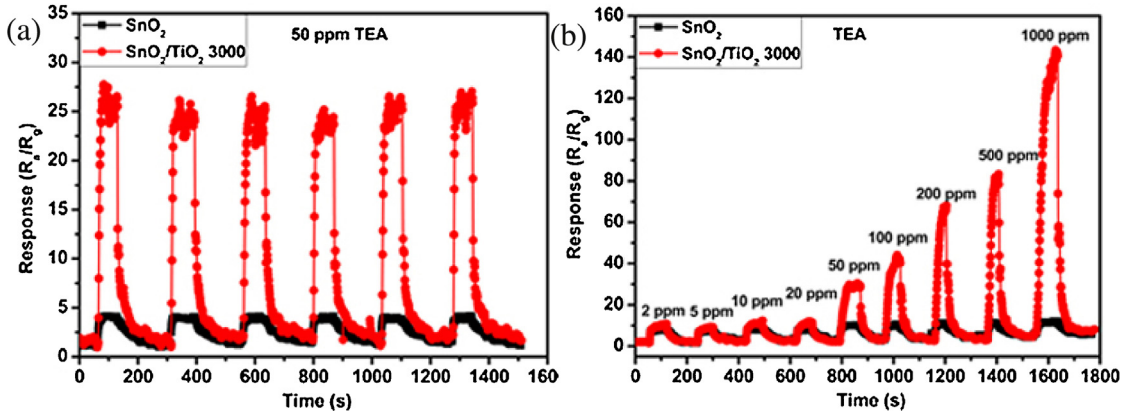

Fig. 6. (a) the repeatability testing of the sensors to 50 ppm TEA at 260 °C; (b) relationship between response and different concentrations of TEA at 260 °C.

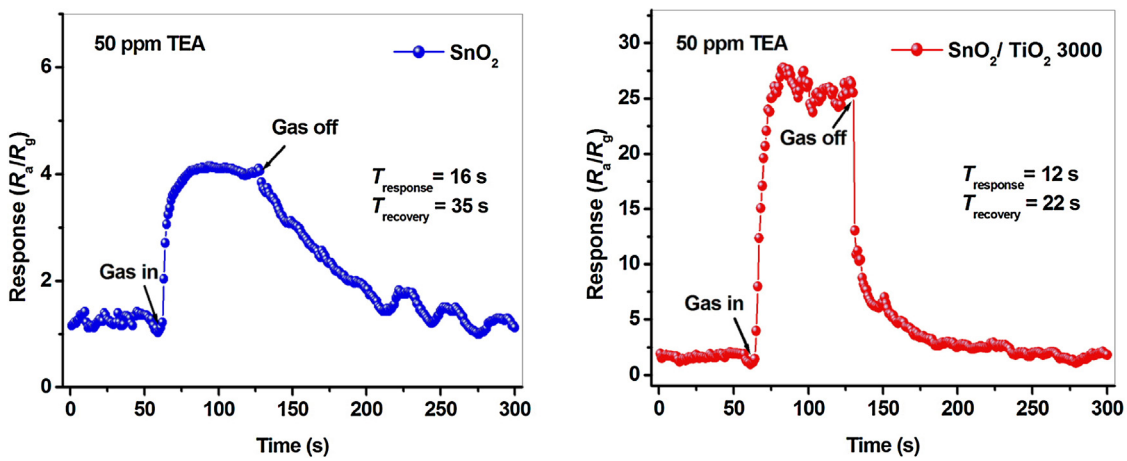

Fig. 7. Response and recovery time of the S and ST3 sensors to 50 ppm TEA at 260 °C. (a) S sensor; (b) ST3 sensor.

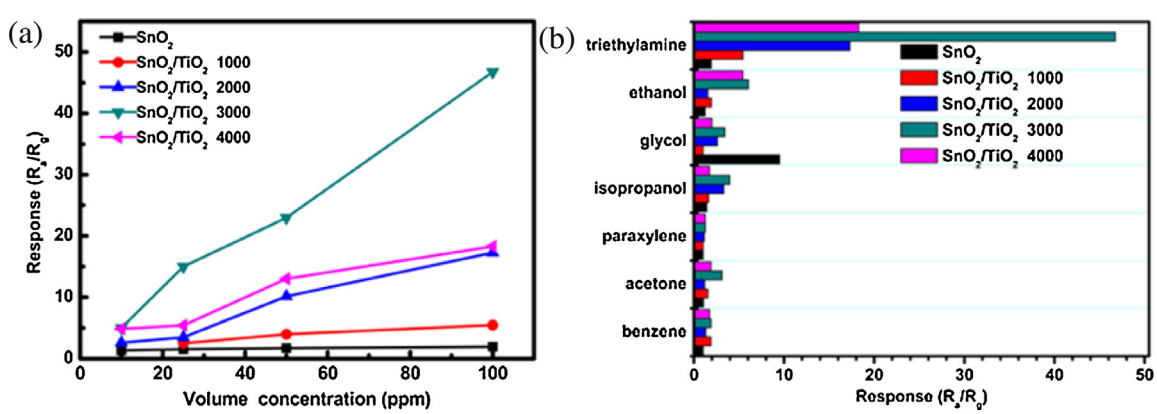

Fig. 8. (a) The corresponding relationship between response and concentration; (b) Selectivity of the sensors for different target gases.

interfering gases is lower than 10 except ethanol. But, the response to TEA is as high as 47. This indicates an excellent selectivity to TEA. The reason may be the different reaction activity of target gases in terms of bond energy [41,42]. The main bond energies of target gases, for example, TEA (C-N), isopropanol (C-C), ethanol (O-H), benzene (C=C), and acetone (C=O), are 307, 345, 458.8, 610.3, and 798.9 kJ/mol, respectively [41,42]. Due to the low C-N bond energy, the high reaction activity of TEA molecules is expected to contribute to the high response of TiO_2/SnO_2 nanosheets sensors. Moreover, the response values of ST sensors are higher than those of S sensor, especially to TEA. The maximum response of ST3 sensor to TEA is about 24 times higher than the pure SnO_2 nanosheet sensor, which is very attractive for trace TEA detection. A comparison between the sensing performances of our sensor and literature results is summarized in Table 1. It is worth noting that the ST3 sensor in this work exhibits better sensing properties in comparison with those reported in the literature.

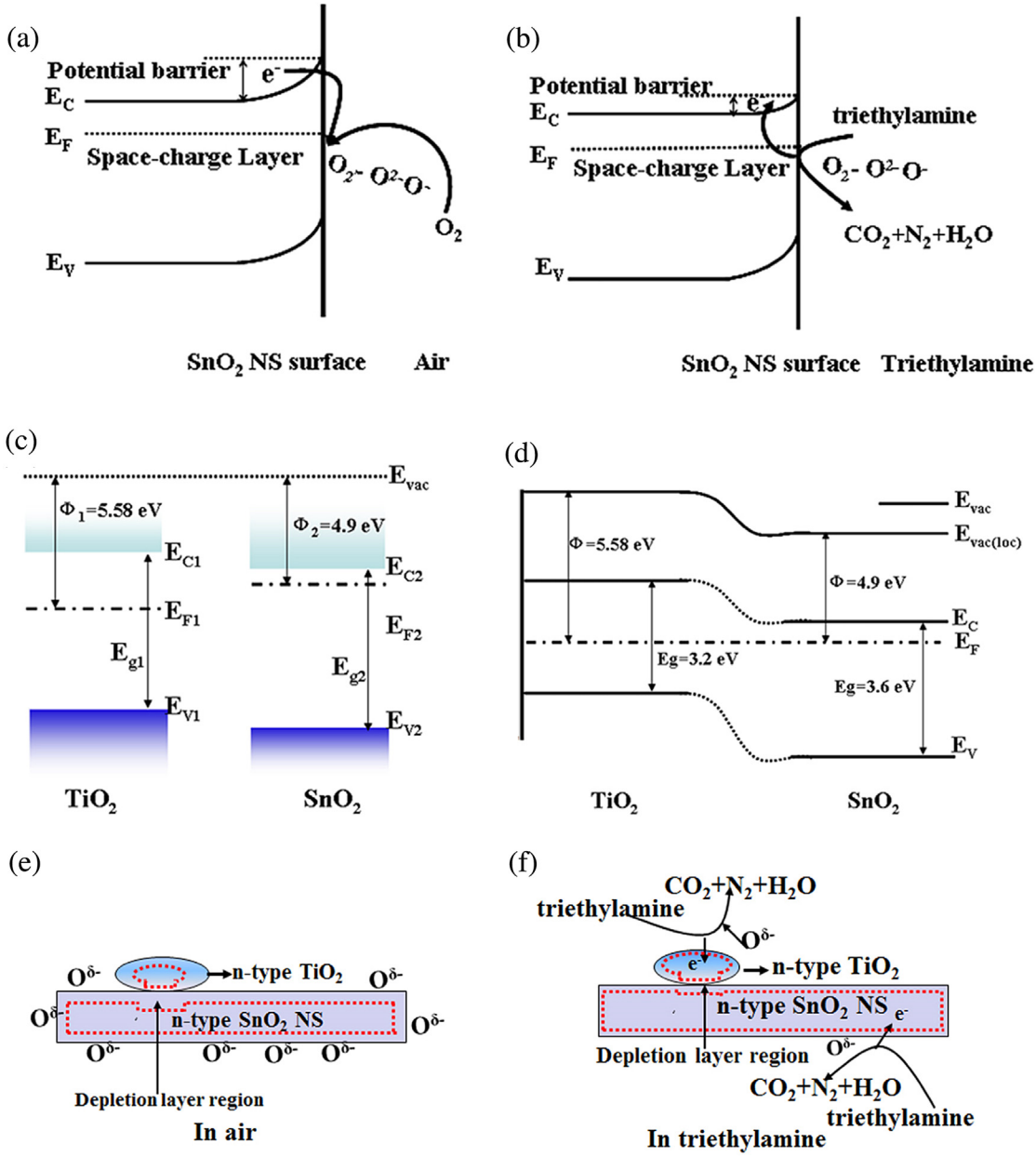

Fig. 9. (a and b) The energy band diagram of SnO_2 nanosheet in air and in TEA; (c and d) The energy band diagram of n-type TiO_2 and n-type SnO_2 heterostructure. (e and f) Schematic model for the TiO_2/SnO_2 n–n heterojunction nanosheets sensor exposed to air and TEA gas, respectively. The outside part indicated by red dashed lines is the depletion layer.

Table 1
Sensing properties of TiO_2/SnO_2 nanosheets and other reported gas sensors working under different operating temperatures.

Sensing material	[TEA] (ppm)	T_{sens} (°C)	Response (R_a/R_g)	Refs.
SnO_2 nanorods	50	350	65	[20]
SnO_2 flowerlike	100	350	4	[39]
brick-shaped SnO_2	100	160	70	[40]
TiO_2/SnO_2 nanosheets	100	260	52.3	Our work

3.3. Mechanism on enhanced ST sensing properties

The sensing mechanism of n-type semiconductor sensors has been well explained by the space-charge layer mode [20,43,44]. The change of resistance can be primarily ascribed to the adsorption and desorption of the target gas molecules on the surface of the sensing materials. Once the SnO_2-based sensing materials are exposed to air at a high temperature, oxygen molecules adsorb on the SnO_2 surface and extract electrons in the bulk to become oxygen ions species (O_2^-, O^{2-}, or O^-), which causes the formation of depletion layer in the surface of sensing materials. Therefore, the decrease of the carrier concentration leads to a high resistance of the sensor. When the SnO_2 nanosheets are exposed to TEA gas, the target molecules will react with the oxygen ions, which results in electrons being released to the depletion layer of SnO_2 and increases the carrier concentration of SnO_2. The working principles in air and target gas are schematically shown in Fig. 9(a–b).

However, after the loading of TiO_2 nanoparticles, the sensing mechanism will become complex due to the formation of n–n heterojunctions. The improvement of the sensing properties to TEA gas may be attributed to the interface between SnO_2 and TiO_2, which means the formation of n–n heterojunctions between SnO_2 nanosheets and TiO_2 nanoparticles [45]. Fig. 9(c–d) shows the

energy band structure diagram of n-type SnO_2/n-type TiO_2 heterocontact. As we know, the work functions of TiO_2 and SnO_2 have been reported to be 5.58 and 4.9 eV, respectively [46–49]. When the TiO_2 is in contact with SnO_2, noticeable electron transfer from SnO_2 to TiO_2 will occur and the charge transfer leads to band bending around surface due to the large gradient of the band gap and work function [50,51]. This creates an electron depletion layer on the side of SnO_2 and further bends the energy band and leads to a higher resistance of sensing materials than of the pure SnO_2 sensor. In addition, the capture of the electrons occurs in the two materials residing in both TiO_2 and SnO_2 near their interface. This carrier capture would create depletion layers in both the TiO_2 and SnO_2 near the interface and a potential barrier at the TiO_2-SnO_2 interface. Therefore, when TiO_2/SnO_2 nanostructures are formed, the electrons in SnO_2 are greatly depleted due to the formation of n–n heterojunctions in addition to the adsorption of oxygen molecules, as shown in Fig. 9(e).

However, once TiO_2/SnO_2 sensors are exposed to reducing TEA gas, the interaction of TEA molecules with pre-adsorbed oxygen ions releases electrons back to TiO_2/SnO_2 nanosheets. The reaction between TEA and surface oxygen species can be simply described as [47,52,53]

$$(C_2H_5)_3N + O^{\delta-} \leftrightarrow CO_2 + H_2O + NO_2 + e^-$$

This significantly reduces the width of the depletion layer between TiO_2 and SnO_2, resulting in a great decrease in sensor resistance, shown in Fig. 9(f). In brief, in comparison with the S sensor, the formation of n–n heterojunction in ST sensor greatly increases the resistance in air and decreases the resistance in TEA gas. Thus, based on the definition of sensor response ($S = R_a/R_g$), the enhanced S to TEA is mainly attributed to the variation of resistance caused by the formation of n–n junction.

4. Conclusions

In conclusion, we manufactured a highly sensitive and selective TEA gas sensor based on TiO_2/SnO_2 n–n heterojunctions. The TiO_2/SnO_2 nanosheet gas sensor exhibits highly sensitive and selective sensing property to TEA gas. The as-prepared ST3 sensor response could reach 52.3 when exposed to 100 ppm TEA gas, which is much higher than that of pure SnO_2 nanosheet sensor. Compared with the pure SnO_2 sensor (S sensor), the depletion layer formed at the n–n heterojunctions in ST sensor greatly increases the change of the resistance in air and in TEA gas, which leads to a high response to TEA gas. This theoretical model can also be used to explain other n-n heterojunctions for sensor application. This work provides a rational way for designing high performances gas sensors.

Acknowledgments

This work is supported by Shandong Provincial Science Foundation (No.ZR2014JL045 and ZR2015BQ006) and University of Jinan Science Foundation (No. XKY1504).

Appendix A. Supplementary data

Supplementary data associated with this article can be found, in the online version, at http://dx.doi.org/10.1016/j.snb.2016.01.059.

References

[1] L. Xu, H.J. Song, J. Hu, Y. Lv, K.L. Xu, A cataluminescence gas sensor for triethylamine based on nanosized LaF_3–CeO_2, Sens. Actuators B 169 (2012) 261–266.
[2] D.X. Ju, H.Y. Xu, Q. Xu, H.B. Gong, Z.W. Qiu, J. Guo, J. Zhang, B.Q. Cao, High triethylamine-sensing properties of NiO/SnO_2 hollow sphere P–N heterojunction sensors, Sens. Actuators B 215 (2015) 39–44.
[3] J.F. Haskin, G.W. Warren, L.J. Priestley, Gas chromatography determination of constituents in the study of azeotropes, Anal. Chem. 30 (1958) 217–219.
[4] W.M. Moore, R.J. Edwards, L.T. Bavda, An improved capillary gas chromatography method for triethylamine: application to sarafloxacin hydrochloride and GnRH residual solvents testing, Anal. Lett. 32 (1999) 2603–2612.
[5] W.H. Zhang, W.D. Zhang, Fabrication of SnO_2–ZnO nanocomposite sensor for selective sensing of trimethylamine and the freshness of fishes, Sens. Actuators B 134 (2008) 403–408.
[6] E. Filippo, D. Mannob, A. Buccolieri, A. Serra, Green synthesis of sucralose-capped silver nanoparticles for fast colorimetric triethylamine detection, Sens. Actuators B 178 (2013) 1–9.
[7] C. Wang, K. Ståhl, H. Huang, Y. Zhong, J.Z. Jiang, Ultrathin SnO_2 nanosheets: oriented attachment mechanism, nonstoichiometric defects, and enhanced lithium-ion battery performances, J. Phys. Chem. C 116 (2012) 4010–4011.
[8] H.Y. Xu, X.Q. Chen, J. Zhang, J.Q. Wang, B.Q. Cao, D.L. Cui, NO_2 gas sensing with SnO_2–ZnO/PANI composite thick film fabricated from porous nanosolid, Sens. Actuators B 176 (2013) 166–173.
[9] L. Wang, S. Wang, Y. Wang, H. Zhang, Y. Kang, W. Huang, Synthesis of hierarchical SnO_2 nanostructures assembled with nanosheets and their improved gas sensing properties, Sens. Actuators B 188 (2013) 85–93.
[10] C. Burda, X. Chen, R. Narayanan, M.A. El-Sayed, Chemistry and properties of nanocrystals of different shapes, Chem. Rev. 105 (2005) 1025–1112.
[11] X.H. Liu, J. Zhang, X.Z. Guo, S.H. Wu, S.R. Wang, Enhanced sensor response of Ni-doped SnO_2 hollow spheres, Sens. Actuators B: Chem. 152 (2011) 162–167.
[12] H.Y. Xu, D.L. Cui, B.Q. Cao, Effect of nanoparticle size on gas-sensing properties of tin dioxide sensors, Chem. Res. Chin. Univ. 28 (6) (2012) 1086–1090.
[13] B. Cheng, J.M. Russell, W.S. Shi, L. Zhang, E.T. Samulski, Large-scale, solution phase growth of single-crystalline SnO_2 nanorods, J. Am. Chem. Soc. 126 (2004) 5972–5973.
[14] M.H. Xua, F.S. Cai, J. Yin, Z.H. Yuan, L.J. Bie, Facile synthesis of highly ethanol-sensitive SnO_2 nanosheets using homogeneous precipitation method, Sens. Actuators B 145 (2010) 875–878.
[15] L. Wang, T. Fei, Z. Lou, T. Zhang, Three-dimensional hierarchical flowerlike α-Fe_2O_3 nanostructures: synthesis and ethanol-sensing properties, ACS Appl. Mater. Interfaces 3 (2011) 4689–4694.
[16] P. Sun, Y. Cao, J. Liu, Y. Sun, J. Ma, G. Lu, Dispersive SnO_2 nanosheets: hydrothermal synthesis and gas-sensing properties, Sens. Actuators B 156 (2011) 779–783.
[17] C.S. Moon, H.R. Kim, Highly sensitive and fast responding CO sensor using SnO_2 nanosheets, Sens. Actuators B 131 (2008) 556–564.
[18] J.Y. Jung, C.S. Lee, Characteristics of the TiO_2/SnO_2 thick film semiconductor gas sensor to determine fish freshness, J. Ind. Eng. Chem. 17 (2011) 237–242.
[19] E. Nikana, A. Ali Khodadadi, Y. Mortazavi, Highly enhanced response and selectivity of electrospun ZnO-doped SnO_2 sensors to ethanol and CO in presence of CH_4, Sens. Actuators B 184 (2013) 196–204.
[20] D. Wang, X.F. Chu, M.L. Gong, Gas-sensing properties of sensors based on single-crystalline SnO_2 nanorods prepared by a simple molten-salt method, Sens. Actuators B 117 (2006) 183–187.
[21] X.H. Liu, J. Zhang, X.Z. Guo, S.R. Wang, S.H. Wu, Core–shell α-Fe_2O_3@SnO_2/Au hybrid structures and their enhanced gas sensing properties, RSC Adv. 2 (2012) 1650–1655.
[22] J. Zhang, X.H. Liu, L.W. Wang, T.L. Yang, X.Z. Guo, S.H. Wu, Synthesis and gas sensing properties of alpha-Fe_2O_3@ZnO core–shell nanospindles, Nanotechnology 22 (2011) 1264–1270.
[23] C.L. Hsu, Y.D. Gao, Y.S. Chen, T.J. Hsueh, Vertical Ti doped ZnO nanorods based on ethanol gas sensor prepared on glass by furnace system with hotwire assistance, Sens. Actuators B 192 (2014) 550–557.
[24] D.X. Ju, H.Y. Xu, Z.W. Qiu, J. Guo, J. Zhang, B.Q. Cao, Highly sensitive and selective triethylamine-sensing properties of nanosheets directly grown on ceramic tube by forming NiO/ZnO PN heterojunction, Sens. Actuators B 200 (2014) 288–296.
[25] L. Wang, H. Dou, Z. Lou, T. Zhang, Encapsuled nanoreactors (Au@SnO_2): a new sensing material for chemical sensors, Nanoscale 5 (2013) 2686–2691.
[26] B. Lyson-Sypien, A. Czapla, M. Lubecka, P. Gwizdza, K. Schneider, K. Zakrzewska, K. Michalowb, T. Grauleb, A. Reszka, M. Rekas, A. Lacz, M. Radecka, Nanopowders of chromium doped TiO_2 for gas sensors, Sens. Actuators B 175 (2012) 163–172.
[27] X.G. Li, X.X. Li, J. Wang, S.W. Lin, Highly sensitive and selective room-temperature formaldehyde Sensors using hollow TiO_2 microspheres, Sens. Actuators B 219 (2015) 158–163.
[28] A. Hazra, S.K. Hazra, E. Bontempi, V.N. Lakshmi, S. Sinha, C.K. Sarkar, S. Basu, Anodically grown nanocrystalline titania thin film for hydrogen gas sensors—a comparative study of planar and MAIM device configurations, Sens. Actuators B 188 (2013) 787–796.
[29] J. Deng, B. Yu, Z. Lou, L. Wang, R. Wang, T. Zhang, Facile synthesis and enhanced ethanol sensing properties of the brush-like ZnO–TiO_2 heterojunctions nanofibers, Sens. Actuators B 184 (2013) 21–26.
[30] Y. Zeng, L. Qiao, Y.F. Bing, M. Wen, B. Zou, W. Tao Zheng, T. Zhang, G.T. Zou, Development of microstructure CO sensor based on hierarchically porous ZnO nanosheet thin films, Sens. Actuators B 173 (2012) 897–902.

[31] O. Lupan, L. Chow, Growth of tetragonal SnO_2 microcubes and their characterization, J. Cryst. Growth 311 (2008) 152–155.
[32] F. Hernandez-Ramirez, J.D. Prades, Insight into the role of oxygen diffusion in the sensing mechanisms of SnO_2 nanowires, Adv. Funct. Mater. 18 (2008) 2990–2994.
[33] A.A. Firooz, A.R. Mahjouba, Effects of flower-like, sheet-like and granular SnO_2 nanostructures prepared by solid-state reactions on CO sensing, Mater. Chem. Phys. 115 (2009) 196–199.
[34] C.S. Moon, H.-R. Kim, Highly sensitive and fast responding CO sensor using SnO_2 nanosheets, Sens. Actuators B 131 (2008) 556–564.
[35] Y. Masuda, T. Ohji, K. Kato, Tin oxide nanosheet assembly hydrophobic/hydrophilic coating and cancer sensing, ACS Appl. Mater. Interfaces 4 (2012) 1666–1674.
[36] M. Kwoka, L. Ottaviano, M. Passacantando, S. Santucci, G. Czempik, J. Szuber, XPS study of the surface chemistry of L-CVD SnO_2 thin films after oxidation, Thin Solid Films 490 (2005) 36–42.
[37] L.J. Bie, X.N. Yan, J. Yin, Y.Q. Duan, Z.H. Yuan, Nanopillar ZnO gas sensor for hydrogen and ethanol, Sens. Actuators B 126 (2007) 604–608.
[38] D.X. Ju, H.Y. Xu, J. Zhang, J. Guo, B.Q. Cao, Direct hydrothermal growth of ZnO nanosheets on electrode for ethanol sensing, Sens. Actuators B 201 (2014) 444–451.
[39] B. Liu, L.H. Zhang, H. Zhao, Y. Chen, H.Q. Yang, Synthesis and sensing properties of spherical flowerlike architectures assembled with SnO_2 submicron rods, Sens. Actuators B 173 (2012) 643–651.
[40] Y.J. Xie, J.P. Du, R.H. Zhao, H.Y. Wang, H.L. Yao, Facile synthesis of hexagonal brick-shaped SnO_2 and its gas sensing toward triethylamine, J. Environ. Chem. Eng. 1 (2013) 1380–1384.
[41] H.Y. Xu, D.X. Ju, W.R. Li, H.B. Gong, J. Zhang, J.Q. Wang, B.Q. Cao, Low-working-temperature, fast-response-speed NO_2 sensor with nanoporous-SnO_2/polyaniline double-layered film, Sens. Actuators B 224 (2016) 654–660.
[42] L.X. Zhang, J.H. Zhao, H.Q. Lu, L. Li, J.F. Zheng, J. Zhang, H. Li, Z.P. Zhu, Highly sensitive and selective dimethylamine sensors based on hierarchical ZnO architectures composed of nanorods and nanosheet-assembled microspheres, Sens. Actuators B 171–172 (2012) 1101–1109.
[43] L. Wang, J. Deng, Z. Lou, T. Zhang, L. Wang, Cross-linked p-type Co_3O_4 octahedral nanoparticles in 1D n-type TiO_2 nanofibers for high-performance sensing devices, J. Mater. Chem. A 2 (2014) 10022–10028.
[44] H.C. Chiu, C.S. Yeh, Hydrothermal synthesis of SnO_2 nanoparticles and their gas-sensing of alcohol, J. Phys. Chem. C 111 (2007) 7256–7259.
[45] R.N. Bulakhe, S.V. Patil, P.R. Deshmukh, N.M. Shinde, C.D. Lokhande, Fabrication and performance of polypyrrole (Ppy)/TiO_2 heterojunction for room temperature operated LPG sensor, Sens. Actuators B 181 (2013) 417–423.
[46] H. Liu, X. Sun, M. Sun, Y. Zhang, B. Xue, Y. Liu, First-principles calculation on the band structure of Co-doped anatase TiO_2, J. Chin. Ceramic Soc. 5 (2011) 1617–1621.
[47] E.K. Liu, B.S. Zhu, J.S. Luo, The Physics of Semiconductors, 7th ed., Publishing house of electronics industry, Beijing, 2011, pp. 243–244.
[48] S.M. Sze, N.K. Kwok, Physics of Semiconductor Devices, A John Wiley & Sons, 2007, pp. 127–130, Jnterscience.
[49] D. Ju, H. Xu, Z. Qiu, Z. Zhang, Q. Xu, J. Zhang, J. Wang, B. Cao, Near room temperature, fast-response, and highly sensitive triethylamine sensor assembled with Au-loaded ZnO/SnO_2 core–shell nanorods on flat alumina substrates, ACS Appl. Mater. Interfaces 7 (2015) 19163–19171.
[50] A. Kusior, M. Radecka, Ł. Zych, K. Zakrzewska, A. Reszka, B.J. Kowalski, Sensitization of TiO_2/SnO_2 nanocomposites for gas detection, Sens. Actuators B 189 (2013) 251–259.
[51] L. Ma, H. Fan, H. Tian, J. Fang, X. Qian, The n-ZnO/n-In_2O_3 heterojunction formed by a surface-modification and their potential barrier-control in methanal gas sensing, Sens. Actuators B 222 (2016) 508–516.
[52] J. Wang, L. Yu, H. Wang, S. Ruan, J. Li, F. Wu, Preparation and triethylamine sensing properties of Ce doped In_2O_3 nanofibers, Acta Physico–Chimica Sinica 26 (2010) 3105.
[53] Y. Takao, M. Nakanishi, T. Kawaguchi, Y. Shimizu, M. Egashira, Semiconductor dimethylamine gas sensors with high sensitivity and selectivity, Sens. Actuators B 24–25 (1995) 375–379.

Biographies

Hongyan Xu received her Ph.D. degree from State Key Lab of Crystal Materials, Shandong University in 2006. Now she is an Associate Professor at School of Materials Science and Engineering, University of Jinan. Her main research interests are the synthesis and fabrication of semiconductor nano-materials and high performance conductive polymer composite chemical gas sensors.

Judianxing Ju is currently studying for the M.S. degree in the Department of material science and Engineering, University of Jinan, China. Now his research interests focus on the nanostructured semiconductor materials for the gas sensor applications.

Wenru Li graduated from school of materials science and engineering, University of Jinan in 2015. Now he is a graduate student focusing on gas sensing materials for master degree the same university.

Jun Zhang received his Ph.D. degree from the Department of Chemistry, Nankai University in 2011. Now he is working at School of Materials Science and Engineering, University of Jinan. His main research interest is gas sensing materials.

Jieqiang Wang received his Ph.D. degree from Northeastern University in 1999. Now he works as a Professor at School of Materials Science and Engineering, University of Jinan. His researchs focus on the synthesis and fabrication of semiconductor nano-materials.

Bingqiang Cao received the Ph.D. degree from the Institute of Solid State Physics, Chinese Academy of Sciences (CAS) in 2006. After that, he worked as a postdoctoral researcher at University of Leipzig from September 2006 to August 2008, and then as a JSPS fellow at Kyushu University from August 2008 to July 2009. Now, he is a Principle Investigator and Oversea Taishan Scholar endowed professor of University of Jinan in China. His research is focused on nanostructures, heterostructures, thin films, and transparent optoelectrical devices based on inorganic semiconductors.